



# Electric double-layer capacitance between an ionic liquid and few-layer graphene

Eri Uesugi<sup>1</sup>, Hidenori Goto<sup>1,2</sup>, Ritsuko Eguchi<sup>1</sup>, Akihiko Fujiwara<sup>3</sup> & Yoshihiro Kubozono<sup>1,2</sup>

<sup>1</sup>Research Laboratory for Surface Science, Okayama University, Okayama 700-8530, Japan, <sup>2</sup>Research Centre of New Functional Materials for Energy Production, Storage and Transport, Okayama University, Okayama 700-8530, Japan, <sup>3</sup>Japan Synchrotron Radiation Research Institute, SPring-8, Hyogo 679-5198, Japan.

SUBJECT AREAS:  
SURFACES, INTERFACES  
AND THIN FILMS  
APPLIED PHYSICS  
ELECTRONIC PROPERTIES AND  
MATERIALS  
ELECTRONIC PROPERTIES AND  
DEVICES

Received  
27 November 2012

Accepted  
15 March 2013

Published  
3 April 2013

Correspondence and  
requests for materials  
should be addressed to  
H.G. ([p57f8bcq@cc.okayama-u.ac.jp](mailto:p57f8bcq@cc.okayama-u.ac.jp))

Ionic-liquid gates have a high carrier density due to their atomically thin electric double layer (EDL) and extremely large geometrical capacitance  $C_g$ . However, a high carrier density in graphene has not been achieved even with ionic-liquid gates because the EDL capacitance  $C_{EDL}$  between the ionic liquid and graphene involves the series connection of  $C_g$  and the quantum capacitance  $C_q$ , which is proportional to the density of states. We investigated the variables that determine  $C_{EDL}$  at the molecular level by varying the number of graphene layers  $n$  and thereby optimising  $C_q$ . The  $C_{EDL}$  value is governed by  $C_q$  at  $n < 4$ , and by  $C_g$  at  $n > 4$ . This transition with  $n$  indicates a composite nature for  $C_{EDL}$ . Our finding clarifies a universal principle that determines capacitance on a microscopic scale, and provides nanotechnological perspectives on charge accumulation and energy storage using an ultimately thin capacitor.

Single-layer graphene (SLG) has two kinds of singularities. One is a topological singularity at  $K$  points in non-doped SLG, called the Dirac point. The carrier transport at the Dirac point, with a vanishing density of states  $D(E)$ , has been intensively studied<sup>1–5</sup>. The other is the van Hove singularity at  $M$  points in highly doped SLG, which has recently attracted significant attention due to predictions of several novel phenomena such as superconductivity<sup>6,7</sup>, ferromagnetism<sup>8</sup>, and charge/spin density waves<sup>9,10</sup> caused by divergent  $D(E)$  and a band structure with high symmetry. We can reach this state by doping SLG with 0.25 electrons or holes per carbon atom ( $\sim 1 \times 10^{15}/\text{cm}^2$ ). This high carrier density is expected to be attainable with an ionic-liquid gate because of its thin electronic double layer (EDL)<sup>11–14</sup>, *i.e.* large geometrical capacitance determined by  $C_g = \epsilon_{\text{IL}} \epsilon_0 / d$ . Here,  $\epsilon_{\text{IL}}$ ,  $\epsilon_0$  and  $d$  are the relative permittivity of the ionic liquid, vacuum permittivity, and thickness of EDL, respectively. However, studies have demonstrated that carrier doping into SLG with ionic liquids is much lower than expected<sup>15,16</sup>. This is because the potential difference between an ionic liquid and SLG is made smaller than the applied gate voltage  $V_g$  by the shift of the Fermi energy  $E_F$  when doping SLG with an additional charge of  $Q$ . This phenomenon can be interpreted in terms of the quantum capacitance  $C_q$ , defined as  $C_q = eQ/E_F = e^2 D(E_F)$ <sup>15,17,18</sup>, which is connected to  $C_g$  in series. Thus, the total capacitance  $C_{EDL}$  between the ionic liquid and SLG is understood as follows:

$$1/C_{EDL} = 1/C_g + 1/C_q \quad (1)$$

The effect of  $C_q$  is prominent when  $C_q \ll C_g$ , which is characteristic of the combination of SLG with small  $C_q$  and an ionic liquid with a large  $C_g$ . Thus, even if an ionic liquid has a large  $C_g$ , small  $C_q$  limits  $C_{EDL}$  to make high charge density unattainable. Here, increasing the layer number  $n$  might solve this problem, because  $D(E)$  increases with  $n$ , and accordingly  $C_q$  increases. To find an optimal  $n$  for carrier doping with an ionic liquid is thus quite important for the discovery of novel ordered states in graphene. In addition, the  $C_{EDL}$  will increase with  $n$ , but the specific surface area (the surface area per unit of mass) of few-layer graphene (FLG) decreases. In a practical viewpoint to realise the superior characteristics in graphene-based supercapacitor<sup>19,20</sup>, therefore, it is of significance to elucidate the optimal  $n$  producing both the large  $C_{EDL}$  and specific surface area. In this letter, we examine the capacitance of SLG and FLG while systematically changing  $n$ .

## Results

Our results are summarized in Figs. 1a and 1b. The capacitance  $C_{EDL}$  between the ionic liquid and FLG was measured as a function of  $n$  by two methods, a transport measurement using graphene field effect transistors (FETs) (Fig. 1a), and a capacitance measurement using AC (Fig. 1b). When the gate voltage  $V_g$  induces the charge

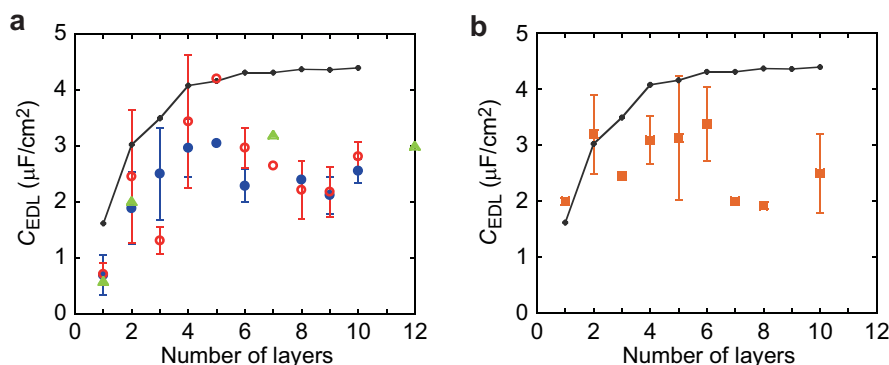


**Figure 1** | Layer-number dependence of EDL capacitance between graphene and ionic liquid (a),  $C_{EDL}$  evaluated from conductivity measurements (Fig. 2 and Supplementary Fig. S2 online) for SLG and FLG devices. The  $C_{EDL}$  values measured in hole-carrier and electron-carrier regimes using two-terminal devices are indicated by blue solid circles and red open circles, respectively. The  $C_{EDL}$  values evaluated from Hall coefficients are indicated by green triangles. (b),  $C_{EDL}$  directly measured with AC (Fig. 3). The minimum  $C_{EDL}$  values from  $V_{tg} = -1$  to  $1$  V are plotted. In (a) and (b), the error bars are the standard deviation of the data measured for each  $n$  device. The black solid lines in (a) and (b) represent calculated  $C_{EDL}$  based on a simple theoretical model (Fig. 4). Dependencies of experimental data on  $n$  are consistent with the model.

$Q(V_g)$ ,  $C_{EDL}^{DC} = Q/V_g$  and  $C_{EDL}^{AC} = dQ/dV_g$  are obtained by the transport and capacitance measurements, respectively. These two measurements are complementary to each other and are especially important in the estimation of  $C_{EDL}$ , which depends significantly on measurement frequency due to the slow transport of the ions in an ionic liquid. The calculated values of  $C_{EDL}$  are also shown in Figs. 1a and 1b, and are in good agreement with the experimental data. At  $n = 1$ , a small  $C_{EDL}$  is observed, as in previous studies<sup>15,16</sup>. With increasing  $n$ ,  $C_{EDL}$  increases and saturates at  $n > 4$ . In the following, we describe the experimental and theoretical details.

First, we evaluated  $C_{EDL}$  from transport measurements. Two-terminal graphene FETs were prepared on SiO<sub>2</sub> 300 nm/highly doped Si substrate. The structure of the device and the optical microscope image are shown in Fig. 2a. In order to obtain a reliable  $n$  dependence, we used only uniform graphene layers without any overlaps of different layers, wrinkles or folds. If the device has overlaps of different layers, the exposure of interstices between the neighbouring graphene layers to the ionic liquid might lead to inaccurate  $n$  and errors in estimation of surface area. The uniformity of graphene layer was clearly confirmed by the optical contrast of micrographs<sup>16,21–24</sup>. Raman spectroscopy mapping and atomic force microscope (AFM) image also evidenced the uniformity of the graphene layer. The number of devices used in this measurement is shown in Table 1; good reproducibility was obtained. The sheet conductivity  $\sigma$  was measured as a function of back gate voltage  $V_{bg}$  applied to the Si substrate. Next, a droplet of ionic liquid was placed on the graphene surface, and  $\sigma$  was measured again as a function of the top gate voltage  $V_{tg}$  applied to the ionic liquid with a Pt wire (100  $\mu$ m in diameter). In Figs. 2b–2d,  $\sigma$ s of FLG FETs with  $n = 1, 4$ , and  $9$  are plotted as functions of  $V_{bg}$  and  $V_{tg}$ . Note that the horizontal scales are different for  $V_{bg}$  and  $V_{tg}$ . It was found that  $\sigma$  was modulated with a lower gate voltage for  $V_{tg}$  than  $V_{bg}$ . The conductivity varied with gate voltage in proportion to the capacitance as follows,  $|d\sigma/dV_{tg}| = C_{EDL}\mu_{tg}$  or  $|d\sigma/dV_{bg}| = C_{bg}\mu_{bg}$ , where  $\mu$  is electric field mobility and the subscript tg (bg) means top (back) gate. Thus,  $C_{EDL}$  is given by

$$C_{EDL} = \frac{d\sigma/dV_{tg} \mu_{bg}}{d\sigma/dV_{bg} \mu_{tg}} C_{bg} \quad (2)$$

Here,  $d\sigma/dV_{tg(bg)}$  is defined as the steepest slope of the experimental data around the charge neutrality point. Assuming  $\mu_{bg}/\mu_{tg} = 1$  and substituting the experimental value of  $C_{bg} = 11.5$  nF/cm<sup>2</sup>,  $C_{EDL}$  is calculated for each device and plotted in Fig. 1a. A clear  $n$  dependence of  $C_{EDL}$  is found in Fig. 1a.  $C_{EDL}$  is a minimum at  $n = 1$ . With increasing  $n$ ,  $C_{EDL}$  shows a maximum at  $n = 4$  and decreases

smoothly as  $n$  approaches 10. Maximum carrier density was estimated to be  $0.003/C$  atom ( $4.7 \times 10^{13}/\text{cm}^2$ ) at  $n = 4$  and  $V_{tg} = 2$  V.

In order to prove the validity of  $C_{EDL}(n)$  obtained by the transport technique, we directly measured the capacitance using AC. The device structure and the optical microscope image are shown in Fig. 3a. Uniform graphene layers are carefully chosen in this measurement. The graphene layer was covered with photoresist except for a region about 15  $\mu$ m square, on which a droplet of the ionic liquid was placed. AC voltage was applied across the interface between the ionic liquid and FLG, and the capacitance  $C_{EDL}$  was evaluated by the out-of-phase components of the detected current.  $C_{EDL}$  was measured with an excitation amplitude of 10 mV at a frequency of 500 Hz and with a superimposed DC bias voltage  $V_{tg}$  ranging from  $-1$  to  $+1$  V. The equivalent circuit of our system is shown in Fig. 3a<sup>16</sup>. Here, it should be noticed that the contact area between the ionic liquid and Pt electrode is much larger than the area between the ionic liquid and FLG. Hence, the impedance of  $C_{Pt}$  is negligible compared to that of  $C_{EDL}$ . This means that  $V_{tg}$  is effectively applied at the interface between the ionic liquid and FLG. Note that  $V_{tg}$  is uniform along this interface, because the impedance of  $C_{EDL}$  ( $\sim 10^8 \Omega$ ) is much larger than the resistance of FLG ( $10^3 - 10^4 \Omega$ ). The measured impedance is typically  $Z \sim 10^6 - 10^8 i \Omega$  at a frequency of 500 Hz. Therefore, the capacitive component dominates the total impedance, showing that  $C_{EDL}$  can be directly determined by the measurement with LCR meter as described in the method section.

In Fig. 3b,  $C_{EDL}$  for  $n = 6$  is plotted as a function of  $V_{tg}$ . We found that  $C_{EDL}$ s for all the devices significantly depended on  $V_{tg}$ , which corresponds to the ambipolar behaviour in  $D(E)$ . Here it is important to notice that  $V_{tg}$  in our experiment may be different from the actual voltage applied to the FLG since the potential drop caused by the interface of the Pt wire is not considered. The accurate dc bias in the electrochemical impedance analysis may be defined as the potential difference from the reference electrode using a three-terminal setup<sup>15</sup>. However, in our devices used in this study, the potential drop at the Pt interface is expected to be so small that applied voltage from the ground is approximately equal to the actual voltage, because the Pt electrode is much wider than the channel region of FLG, as described above. To compare with the transport measurement, the  $C_{EDL}$  for each device, obtained at the charge neutrality point, is plotted as a function of  $n$  in Fig. 1b. Here the charge neutrality point is defined as the  $V_{tg}$  where  $C_{EDL}$  exhibited the lowest value, and is located around  $V_{tg} = 0$  V as shown in Fig. 3b. Since  $V_{tg} \sim 0$  V, the value of minimum capacitance is obtained without any ambiguities of the bias voltage. Consequently, the discussion on  $n$  dependence of capacitance shown in Fig. 1b is appropriate. As shown in Figs. 1a and

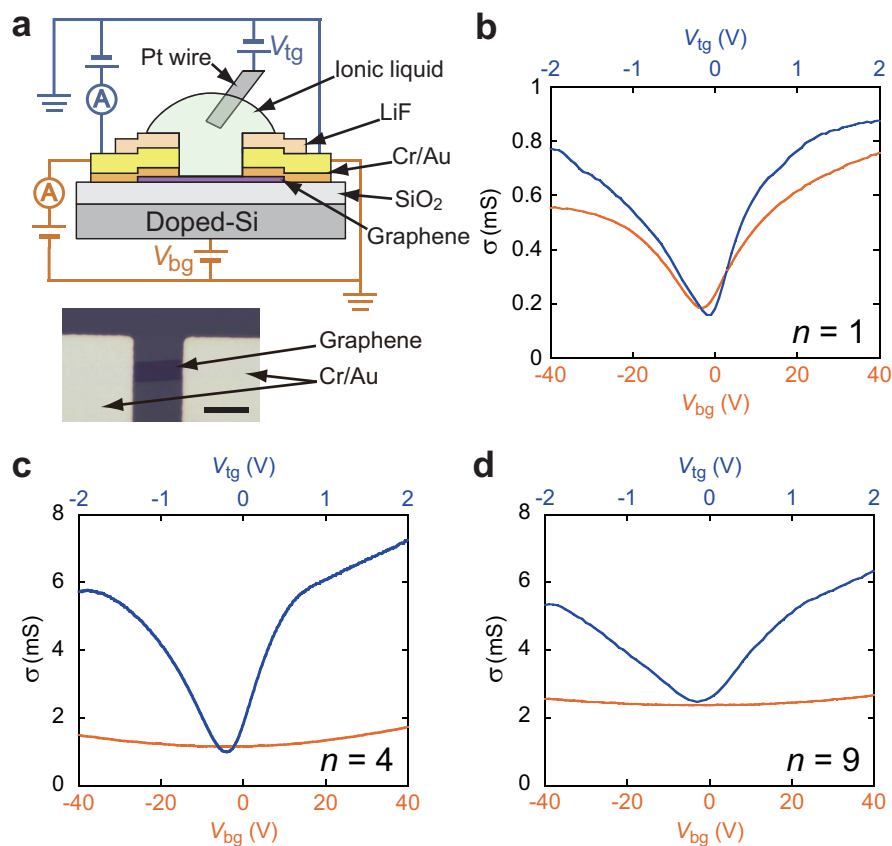


**Figure 2** |  $C_{EDL}$  obtained by 2-terminal transport measurement (a), Schematic side view of two-terminal graphene FET and optical microscope image of a device. Scale bar is 10  $\mu\text{m}$ . Materials and terminal configurations are indicated. After  $\sigma(V_{bg})$  was measured using the circuit shown by orange lines, an ionic liquid was applied and  $\sigma(V_{tg})$  was measured using the circuit shown by blue lines. Actual size of Pt wire (100  $\mu\text{m}$  in diameter) is much larger than the channel length (10  $\mu\text{m}$ ), but it is depicted as a thin wire in the figure for clarity. (b), (c), (d), Comparison of  $\sigma(V_{bg})$  (orange line) and  $\sigma(V_{tg})$  (blue line) for SLG (b), 4-layer (c), and 9-layer graphene (d). Note that the horizontal scales are different for  $V_{bg}$  and  $V_{tg}$ . To determine  $C_{EDL}$  from equation (2), we estimated  $d\sigma/dV_{tg(bg)}$  as the steepest slope of the  $\sigma(V_{tg(bg)})$  curve. The gate voltages were swept from negative to positive values.

1b, a  $C_{EDL} - n$  plot is substantially consistent with that from the transport measurement, which supports the validity of our estimation of  $C_{EDL}$  from the transport measurement.

## Discussion

Here, we discuss the validity of the  $C_{EDL}$  obtained by two-terminal transport measurements. The analysis using equation (2) might oversimplify the estimation of  $C_{EDL}$  because the contribution of  $\mu_{bg}/\mu_{tg}$  is bypassed. First, we consider the validity of the assumption of  $\mu_{bg}/\mu_{tg} = 1$ . This assumption is required because  $C_{EDL}$  and  $\mu_{tg}$  cannot be determined independently without the result of Hall effect. In order to investigate the validity of this assumption, we carried out additional transport measurement using the multi-terminal Hall bar devices with  $n = 1, 2, 7,$  and  $12$ . (see Supplementary Fig. S2 online). In this method, we can independently determine  $C_{EDL}$  and  $\mu_{tg}$  without any assumption. By measuring the Hall coefficient,  $R_H$ , and  $\sigma$  in four-terminal geometry under the gate voltage  $V_g$  ( $V_{bg}$  and  $V_{tg}$ ), we can evaluate  $\mu$  ( $\mu_{bg}$  and  $\mu_{tg}$ ) and  $C$  ( $C_{bg}$  and  $C_{EDL}$ ) independently by using the following equations<sup>25,26</sup>.

$$\mu = |\sigma R_H| \quad (3)$$

$$CV_g = -1/R_H \quad (4)$$

These equations are satisfied in the doped region where only one kind of carrier presents.  $R_H$  was measured as a function of  $V_{tg}$  under perpendicular magnetic field of 6 kOe. The values of  $C_{EDL}$  were estimated from the slope of  $1/R_H - V_{tg}$  curve in the range where

equation (4) holds. The  $C_{EDL} - n$  plot is shown in Fig. S2b and  $C_{EDL}$ s are added in the graph in two-terminal measurement (Fig. 1a). This shows a good agreement between the  $C_{EDL}$  values obtained from two-terminal transport with assumption of  $\mu_{bg}/\mu_{tg} = 1$  and Hall effect without any assumption. Therefore, this result proves the validity of the assumption of  $\mu_{bg}/\mu_{tg} \sim 1$  in the analysis in two-terminal geometry.

Furthermore, we deduced  $\mu_{bg}$  and  $\mu_{tg}$  separately by substituting both  $R_H$  and  $\sigma$  in four-terminal geometry into equation (3), and evaluated  $\mu_{bg}/\mu_{tg}$ . The result is shown in Fig. S2c. The  $\mu_{bg}/\mu_{tg}$  scarcely depends on  $n$  and is regarded as a constant around 0.5. The difference, 1 and 0.5, in  $\mu_{bg}/\mu_{tg}$  between two analyses described above may be closely associated with the contact resistance. The contact resistance reduces the conductance measured in two-terminal geometry, and this effect becomes more significant in highly doped graphene. Accordingly,  $\mu_{tg}$  in two-terminal measurement could be underestimated, because  $\mu_{tg}$  is estimated in more carrier-accumulated region than  $\mu_{bg}$ , while  $\mu_{tg}$  and  $\mu_{bg}$  evaluated from  $R_H$  and  $\sigma$  measured in four-terminal geometry are not affected by the contact resistance.

| Table 1   Number of FLG devices prepared in this study |   |   |   |   |   |   |   |   |   |          |
|--|---|---|---|---|---|---|---|---|---|----------|
| layer number   | 1 | 2 | 3 | 4 | 5 | 6 | 7 | 8 | 9 | 10 total |
| Transport measurement                                  | 4 | 4 | 4 | 3 | 1 | 5 | 1 | 2 | 3 | 30       |
| Capacitance measurement                                | 1 | 2 | 1 | 4 | 2 | 3 | 1 | 2 | 0 | 18       |

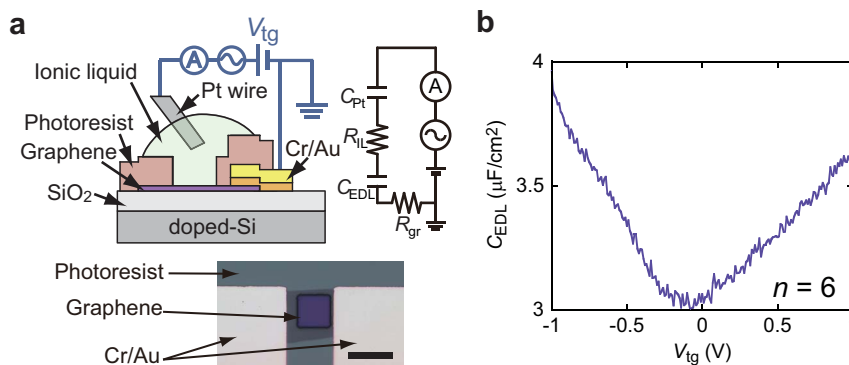


**Figure 3** |  $C_{EDL}$  obtained from direct AC measurement (a), Schematic side view of a device for capacitance measurement and the equivalent circuit. Materials and terminal configurations are indicated.  $R_{IL}$  and  $R_{gr}$  are the electric resistance in the ionic liquid and graphene, respectively.  $C_{Pt}$  is the capacitance between Pt wire and the ionic liquid. Actual size of Pt wire (100  $\mu\text{m}$  in diameter) is much larger than the square window (15  $\mu\text{m}$  on a side), but it is depicted as a thin wire in the figure for clarity. Optical microscope image of a sample is also indicated. Scale bar shows 20  $\mu\text{m}$ . (b),  $V_{tg}$  dependence of  $C_{EDL}$  for 6-layer graphene. The gate voltage was swept from negative to positive values.

This may be one of the reasons why the difference in  $\mu_{bg}/\mu_{tg}$  takes place between two analyses. It is reasonable that  $\mu_{bg}/\mu_{tg}$  using two-terminal mobility enhances from the value ( $\sim 0.5$ ) of  $\mu_{bg}/\mu_{tg}$  estimated from Hall bar devices ( $R_H$  and  $\sigma$  in four-terminal geometry). Thus,  $\mu_{bg}/\mu_{tg}$  in two-terminal geometry can be concluded to be close to unity as we assumed in the analysis of equation (2).

Finally, to give physical meaning to the experimental result, we calculated the charge distribution in the FLG that forms the EDL capacitor, and obtained  $C_{EDL}$  as a function of  $n$ . We define  $U_{EDL}$  ( $= Q^2/2C_{EDL}$ ) as the total energy stored in the EDL capacitor where charges  $+Q$  and  $-Q$  are condensed in the ionic liquid and FLG boundaries, respectively. As shown in Fig. 4a, the charge  $-Q$  is distributed over the layers so as to screen penetration of the electric field into the interior. The electric field  $E_i$  between the  $i$ -th and  $i+1$ -th layer becomes smaller than  $E_{i-1}$  owing to the charge  $-q_i$  lying on the  $i$ -th layer, where  $i = 1, \dots, n$  is numbered from the ionic liquid side. Then,  $C_g$  is obtained by  $C_g = Q^2/2U_g$ , where  $U_g$  is the static field energy due to  $E_i$ :

$$U_g(n) = \frac{1}{2} \sum_{i=0}^{n-1} \epsilon_i \epsilon_0 \int E_i(r)^2 dr = \frac{Q^2 d}{2\epsilon_{IL} \epsilon_0} + \frac{t}{2\epsilon_{gr} \epsilon_0} \sum_{i=1}^{n-1} (Q - \sum_{j=1}^i q_j)^2 \quad (5)$$

where  $\epsilon_{gr} = 5.7$  is the relative permittivity of graphite<sup>27</sup> and  $t = 0.34$  nm is the distance between graphene layers<sup>28</sup>. The first term in the right-side expression shows the classical electric field energy accumulated in EDL and the second term indicates that in  $n$ -layer

graphene. Note that a familiar formula  $C_g = \epsilon_{IL} \epsilon_0 / d$  is obtained for SLG owing to  $n = 1$ . On the other hand, we can relate  $C_q$  to the band filling energy  $U_q$ <sup>29</sup>,  $C_q = Q^2/2U_q$ . Originally  $C_q$  was introduced to explain the incomplete shielding of the electric field effect for a two-dimensional electron gas<sup>17</sup>. We extend this concept to thicker films that can completely screen the electric field by expressing  $U_q$  as a summation of the band-filling energy in each layer;

$$U_q(n) = \sum_{i=1}^n \int_0^{E_{Fi}} ED(E) dE = \sum_{i=1}^n \frac{q_i^2}{2e^2 D} \quad (6)$$

where  $E_{Fi}$  is the Fermi energy of the  $i$ -th layer. For simplicity, we used a constant  $D(E)$  to deduce the second equality. As mentioned before,  $C_q = e^2 D$  is obtained for SLG. We minimized  $U_{EDL}$  ( $= U_g + U_q$ ) with respect to each  $q_i$  of the variational parameters and thereby determined  $U_g$ ,  $U_q$ , and  $U_{EDL}$ . Using these energies, capacitances were deduced.  $C_g$ ,  $C_q$ , and  $C_{EDL}$  are plotted as a function of  $n$  in Fig. 4b. All the capacitances significantly depend on  $n$ :  $C_q$  increases and  $C_g$  decreases with  $n$ , and both capacitances saturate to constant values at  $n \gg 4$ . This saturation behaviour corresponds to the fact that the electric field is screened by the charge distributed within 3–4 layers<sup>29,30</sup> in FLG. Note that the charge distribution over 3–4 layers in FLG significantly reduces  $C_g$  because the effective EDL thickness expands from  $d$  to  $\sim d + \alpha t$ ;  $\alpha$  is on the order of unity and determined by the effective charge distribution. Therefore, even if an ionic liquid with extremely thin  $d$  were used,  $C_g$  could not be increased due to the

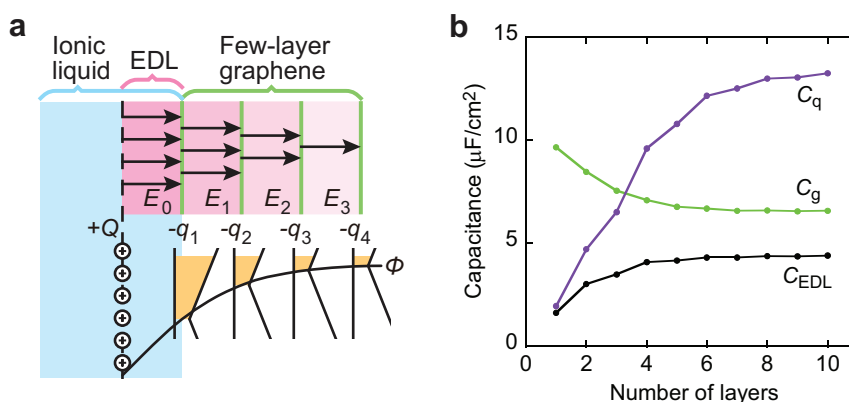


**Figure 4** | Model calculation of  $C_{EDL}$ . (a) Schematic representation of the charge distribution  $-q_i$  in FLG, which shields the electric field. (b) Calculated capacitances as a function of  $n$ . Geometrical capacitance  $C_g$ , quantum capacitance  $C_q$ , and EDL capacitance  $C_{EDL}$  are indicated by green, purple, and black lines, respectively. Details of the calculation can be found in the main text and Supplementary Information. We find that the  $C_{EDL}$  is limited by  $C_q$  for  $n < 4$  and by  $C_g$  for  $n > 4$ .





additional EDL thickness of  $\alpha t$  (see Supplementary Fig. S4 online). Although layered material is considered to be the most suitable for use with an ionic liquid gate, the effect of decreasing  $C_g$  must be taken into account.

In conclusion, we have clarified the microscopic principles determining the capacitance of  $n$ -layer graphene by systematic study. The carrier distribution and the band structure in the electrodes of a capacitor define  $C_g$  and  $C_q$ , respectively, both of which contribute to the total capacitance. This study demonstrates that we may not in principle achieve the high-density carrier accumulation required for  $E_F$  to reach the van Hove singularity even with ionic liquid gated FLG. This result suggests that we need chemical doping<sup>6,31,32</sup> or band control<sup>9</sup> to bring the van Hove singularity close to the Fermi energy. Our finding for EDL capacitor may establish a nanotechnological guideline to improve ultrathin capacitors for charge doping, energy storage, and electric power supply.

## Methods

FLGs were prepared on a SiO<sub>2</sub>/highly doped Si substrate by the micromechanical cleavage of Kish graphite (Covalent Materials Co.). The SiO<sub>2</sub> was 300 nm thick and its surface was coated with a hydrophobic hexamethyldisilazane (HMDS) layer<sup>33</sup> to improve the FET characteristics. The number of graphene layers was distinguished by the contrast of the optical microscope image<sup>16,21–24</sup>, atomic force microscopy (AFM) and Raman spectroscopy<sup>34–37</sup> (see Supplementary Fig. S1 online). As described in the main text, we only used uniform graphene layers without any overlaps of different layers, wrinkles and folds in order to obtain a reliable  $n$  dependence. FLG devices for two-terminal transport measurement were fabricated by photolithography and the vacuum evaporation of metal (Cr 5 nm/Au 50 nm) and insulator (LiF 30 nm) to passivate the electrodes. FLG devices with a Hall bar structure were prepared using the electron beam lithography and oxygen plasma etching. FLG devices for capacitance measurement were coated with 800 nm thick photoresist (Tokyo Oka, TSMR8900) instead of LiF, followed by photolithography to open a window on the graphene layer. All the measurements were carried out in Ar at room temperature. The transport property was measured with a semiconductor device analyser (Agilent B1500A). We evaluated the conductivity from the slope of  $I - V$  curves measured at a drain voltage of  $\pm 1$  mV. Except for the transport measurement using a Hall bar structure, a gel of bmim[PF<sub>6</sub>] was used as the top gate dielectric (preparation details described elsewhere<sup>38</sup>). The geometrical capacitance of this ionic liquid was estimated to be 9.7  $\mu\text{F}/\text{cm}^2$  by extrapolating the measured capacitance at 20 Hz – 100 kHz to 0 Hz. This value corresponds to  $d = 0.6$  nm, assuming  $\epsilon_{\text{IL}} = 7^{15}$ . The capacitance measurement was carried out with a precision LCR meter (Agilent E4980A) applying an AC voltage of 10 mV at 500 Hz and superimposed DC voltage  $V_{\text{lg}}$  from  $-1$  to 1 V. Only the FLG devices with a Hall bar structure were measured by applying  $V_{\text{lg}}$  with an electrolyte LiClO<sub>4</sub>/PEO. The mixing molar ratio of LiClO<sub>4</sub>/PEO is 1/20. The geometrical capacitance of this electrolyte is reported to be 15  $\mu\text{F}/\text{cm}^2$ <sup>39</sup>, which is of the same order as that in bmim[PF<sub>6</sub>].

- Novoselov, K. S. *et al.* Two-dimensional gas of massless Dirac fermions in graphene. *Nature* **438**, 197–200 (2005).
- Du, X., Skachko, I., Barker, A. & Andrei, E. Y. Approaching ballistic transport in suspended graphene. *Nature Nanotech.* **3**, 491–495 (2008).
- Miao, F. *et al.* Phase-coherent transport in graphene quantum billiards. *Science* **317**, 1530–1533 (2007).
- Ando, T. Screening effect and impurity scattering in monolayer graphene. *J. Phys. Soc. Jpn.* **75**, 074716 (2006).
- Adam, S., Hwang, E. H., Galitski, V. M. & Das Sarma, S. A self-consistent theory for graphene transport. *Proc. Natl. Acad. Sci. USA* **104**, 18392–18397 (2007).
- McChesney, J. L. *et al.* Extended van Hove singularity and superconducting instability in doped graphene. *Phys. Rev. Lett.* **104**, 136803 (2010).
- Nandkishore, R., Levitov, L. S. & Chubukov, A. V. Chiral superconductivity from repulsive interactions in doped graphene. *Nature Phys.* **8**, 158–163 (2012).
- Ma, T., Hu, F., Huang, Z. & Lin, H.-Q. Controllability of ferromagnetism in graphene. *Appl. Phys. Lett.* **97**, 112504 (2010).
- Li, G. *et al.* Observation of Van Hove singularities in twisted graphene layers. *Nature Phys.* **6**, 109–113 (2010).
- Makogon, D., van Gelderen, R., Roldán, R. & Smith, C. M. Spin-density-wave instability in graphene doped near the van Hove singularity. *Phys. Rev. B* **84**, 125404 (2011).
- Ueno, K. *et al.* Electric-field-induced superconductivity in an insulator. *Nature Mater.* **7**, 855–858 (2008).
- Ye, J. T. *et al.* Liquid-gated interface superconductivity on an atomically flat film. *Nature Mater.* **9**, 125–128 (2010).
- Bollinger, A. T. *et al.* Superconductor-insulator transition in La<sub>2–x</sub>Sr<sub>x</sub>CuO<sub>4</sub> at the pair quantum resistance. *Nature* **472**, 458–460 (2011).
- Yamada, Y. *et al.* Electrically induced ferromagnetism at room temperature in cobalt-doped titanium dioxide. *Science* **332**, 1065–1067 (2011).
- Xia, J., Chen, F., Li, J. & Tao, N. Measurement of the quantum capacitance of graphene. *Nature Nanotech.* **4**, 505–509 (2009).

- Ye, J. *et al.* Accessing the transport properties of graphene and its multilayers at high carrier density. *Proc. Natl. Acad. Sci. USA* **108**, 13002–13006 (2011).
- Luryi, S. Quantum capacitance devices. *Appl. Phys. Lett.* **52**, 501–503 (1988).
- Das, A. *et al.* Monitoring dopants by Raman scattering in an electrochemically top-gated graphene transistor. *Nature Nanotech.* **3**, 210–215 (2008).
- Lee, S. H. *et al.* Three-dimensional self-assembly of graphene oxide platelets into mechanically flexible macroporous carbon films. *Angew. Chem. Int. Ed.* **49**, 10084–10088 (2010).
- Han, T. H. *et al.* Peptide/graphene hybrid assembly into core/shell nanowires. *Adv. Mater.* **22**, 2060–2064 (2010).
- Blake, P. *et al.* Making graphene visible. *Appl. Phys. Lett.* **91**, 063124 (2007).
- Ni, Z. H. *et al.* Graphene thickness determination using reflection and contrast spectroscopy. *Nano Lett.* **7**, 2758–2763 (2007).
- Oostinga, J. B., Heersche, H. B., Liu, X., Morpurgo, A. F. & Vandersypen, L. M. K. Gate-induced insulating state in bilayer graphene devices. *Nature Mater.* **7**, 151–157 (2008).
- Craciun, M. F. *et al.* Trilayer graphene is a semimetal with a gate-tunable band overlap. *Nature Nanotech.* **4**, 383–388 (2009).
- Novoselov, K. S. *et al.* Electric field effect in atomically thin carbon films. *Science* **306**, 666–669 (2004).
- Ponomarenko, L. A. *et al.* Effect of a High- $\kappa$  Environment on Charge Carrier Mobility in Graphene. *Phys. Rev. Lett.* **102**, 206603 (2009).
- Bechmann, R. *Landolt-Börnstein: Zahlenwerte und Funktionen aus Physik Chemie Astronomie Geophysik und Technik, 6 Auflage II Band 6 Teil, Elektrische Eigenschaften I.* (Springer-Verlag: Berlin, 1959).
- Castro Neto, A. H., Guinea, F., Peres, N. M. R., Novoselov, K. S. & Geim, A. K. The electronic properties of graphene. *Rev. Mod. Phys.* **81**, 109–162 (2009).
- Kuroda, M. A., Tersoff, J. & Martyna, G. J. Nonlinear screening in multilayer graphene systems. *Phys. Rev. Lett.* **106**, 116804 (2011).
- Miyazaki, H. *et al.* Inter-layer screening length to electric field in thin graphite film. *Appl. Phys. Express* **1**, 034007 (2008).
- Xue, M. *et al.* Superconductivity in potassium-doped few-layer graphene. *J. Am. Chem. Soc.* **134**, 6536–6539 (2012).
- Profeta, G., Calandra, M. & Mauri, F. Phonon-mediated superconductivity in graphene by lithium deposition. *Nature Phys.* **8**, 131–134 (2012).
- Lafkioti, M. *et al.* Graphene on a hydrophobic substrate: doping reduction and hysteresis suppression under ambient conditions. *Nano Lett.* **10**, 1149–1153 (2010).
- Ferrari, A. C. *et al.* Raman Spectrum of Graphene and Graphene Layers. *Phys. Rev. Lett.* **97**, 187401 (2006).
- Gupta, A., Chen, G., Joshi, P., Tadigadapa, S. & Eklund, P. C. Raman scattering from high-frequency phonons in supported  $n$ -graphene layer films. *Nano Lett.* **6**, 2667–2673 (2006).
- Graf, D. *et al.* Spatially resolved Raman spectroscopy of single- and few-layer graphene. *Nano Lett.* **7**, 238–242 (2007).
- Malard, L. M., Pimenta, M. A., Dresselhaus, G. & Dresselhaus, M. S. Raman spectroscopy in graphene. *Phys. Rep.* **473**, 51–87 (2009).
- Kaji, Y. *et al.* Characteristics of conjugated hydrocarbon based thin film transistor with ionic liquid gate dielectric. *Organic Electron.* **12**, 2076–2083 (2011).
- Shimotani, H., Asanuma, H., Takeya, J. & Iwasa, Y. Electrolyte-gated charge accumulation in organic single crystals. *Appl. Phys. Lett.* **89**, 203501 (2006).

## Acknowledgments

This work was supported in part by Grants-in-Aid (22244045, 24654105 and 23684028) from MEXT, Japan, by the LEMSUPER project (JST-EU Superconductor Project) and ACT-C project in the Japan Science and Technology Agency (JST), and as a Special Project of Okayama University/MEXT. The transport measurement using Hall bar devices was performed in collaboration with A. Kanda, Y. Ootuka, and K. Tsukagoshi. We are grateful to Y. Takabayashi and T. Kambe for comments and suggestions and to M. Mifune for Raman spectroscopy.

## Author contributions

H. G. and Y. K. planned the experiments. E. U. prepared graphene devices and carried out the transport and capacitance measurements. All authors analysed and discussed the experimental results.

## Additional information

Supplementary information accompanies this paper at <http://www.nature.com/scientificreports>

**Competing financial interests:** The authors declare no competing financial interests.

**License:** This work is licensed under a Creative Commons Attribution-NonCommercial-NoDerivs 3.0 Unported License. To view a copy of this license, visit <http://creativecommons.org/licenses/by-nc-nd/3.0/>

**How to cite this article:** Uesugi, E., Goto, H., Eguchi, R., Fujiwara, A. & Kubozono, Y. Electric double-layer capacitance between an ionic liquid and few-layer graphene. *Sci. Rep.* **3**, 1595; DOI:10.1038/srep01595 (2013).